The Yale Undergraduate Research Journal

Volume 1
Issue 1 *Fall 2020*

Article 13

2020

Designing a Microsecond-Long On-Chip Microwave Delay Line Using SrTiO3 Dielectricity

Kazemi Adachi
Yale University

Mingrui Xu
Yale University

Hong Tang
Yale University

Designing a Microsecond-Long On-Chip Microwave Delay Line Using $SrTiO_3$ Dielectricity

Kazemi Adachi[1], Mingrui Xu[2], Hong Tang[1,2]
[1]Department of Applied Physics, Yale University, [2]Department of Electrical Engineering, Yale University

STEM

ABSTRACT

The delay line is a fundamental circuit design component which slows down a signal with minimal attenuation to provide delay effects, with applications that include interferometry and signal filtering. Cryogenic superconducting delay lines can be less lossy than their regularly conducting counterparts. Scientists can engineer microwave photons with coherence times of several microseconds (μs), longer than current on-chip delays. We utilize the high dielectric constant (>10^4) of strontium titanate at cryogenic temperatures to slow down signal propagation on a coplanar waveguide. Here, we present a design for an on-chip 5 μs superconducting delay line at 5 GHz with small enough footprint to fit on-chip. This delay is more than 200 times longer than previously demonstrated while simultaneously more compact, enabling new regimes of interferometry. We also use simulations to characterize the sensitivity of the optimized design to alternative fabrication parameters. These designs may be useful for quantum information systems and integrated circuit design.

INTRODUCTION

Delay lines are one of the building blocks of circuit design whose function is to introduce a known delay between an input signal and an identical output signal with minimal loss. Using superconductivity in the design of the delay line is particularly attractive because such designs may render loss orders of magnitude lower than that of conventional delay lines. (Talisa et al., 1995) Superconducting delay lines have many potential applications, from electronic warfare and radar systems, (Kapolnek et al., 1993; Liang, Shih, Withers, Cole, & Johansson, 1996) to signal storage and processing systems (Hattori, Yoshitake, & Tahara, 1999) and delay line filters. (Huang, 1997)

As with other delay lines, geometry and design are keys to the performance of superconducting delay lines. A review of superconducting delay line designs including microstrip, stripline, coplanar waveguide (CPW), and conductor-backed (grounded) CPW presents the state of the art in the field. (Su, Wang, Huang, & Lancaster, 2008) There are also different patterns for packing the line onto a wafer including double-spiral, meander line, unit-cell, and other compound designs. The goal of superconducting delay line design is to maximize the delay time on a given wafer area with minimal dispersion and loss. Secondary concerns include maintaining wide bandwidth of functionality. The results are given in centimeters of delay length and nanoseconds of delay time, ultimately rendering a figure of merit of propagation velocity. The longest recorded delay line is a 45 ns delay, achieved on a 4.3 m line—in other words, a propagation velocity of 9.56×10^7 m/s or 0.319. (Hohenwarter, Track, Drake, & Patt, 1993) We propose and computationally verify a delay line design utilizing a high-dielectric medium to achieve a slowdown of more than 200 times with an even smaller footprint. This regime of superconducting delay approaches the limit of microwave photon decoherence time on the order of μs. (Rigetti et al., 2012)

The key to this design is strontium titanate $SrTiO_3$ (hereafter STO). STO is a crystal in the class of ferroelectric perovskites which demonstrate a quantum paraelectric phase transition wherein they develop a spontaneous electric polarization. For STO, this transition means that its dielectric constant goes from around 300 at room temperature to very large values in the tens of thousands below the critical temperature of 4 K. (Müller & Burkard, 1979) For the (001) orientation, it reaches a constant value of 11,000. (Sakudo & Unoki, 1971) Moreover, STO has a very small dielectric loss tangent on the order of 10^{-3} at small temperatures. (Krupka, Geyer, Kuhn, & Hinken, 1994) Lastly, the dielectric constant of STO is voltage tunable. This extra parameter, attributed to the presence

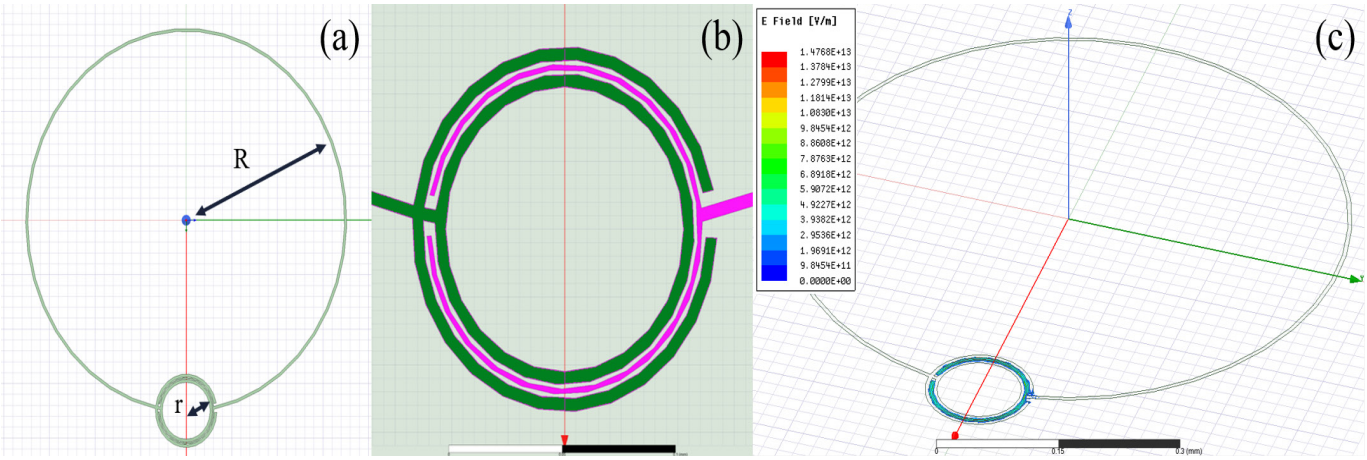

Figure 1. *(a) Ouroboros design with large inductive ring R and small capacitive interlocking rings r. (b) Close-up of interlocking rings. (c) Electric field at resonance is confined to the capacitor of interlocking rings.*

of oxygen vacancies, increases its functionality in embedded devices. (Davidovikj, Manca, van der Zant, Caviglia, & Steele, 2017) Altogether, these factors as well as the significant documentation of other research make STO an optimal choice compared to similar crystals, such as $KTaO_3$. (Krupka et al., 1994) Other high-dielectric constant and low-loss ferroelectric materials have previously been used in phase shifters using delay lines; however, prior investigations with STO have not cooled the STO below 20 K, thus limiting the potential of the characterization. (Jackson et al., 1992) STO has been used in electrically tunable filters (Findikoglu et al., 1996) and resonators, (Adam, Fuchs, & Schneider, 2002) and it may be suitable for future use in microwave domain EM probes.

$SrTiO_3$ CHARACTERIZATION

We began our process by experimentally verifying the quantum paraelectric phase transition of STO, which has been studied theoretically and experimentally for the past several decades. We coupled an STO crystal slab to a microwave resonator by placing the STO flush on top and measuring the resulting change in resonance. In particular, during this process we also sought to characterize the strength of the coupling dependent on the spacing between the STO and the microwave resonator. For our resonator, we used an 'ouroboros' resonator (Han, Zou, & Tang, 2016)—so named because of its resemblance to the Greek symbol of a snake eating its own tail—which is a simple LC resonator. The ouroboros consisted of a "capacitor" formed by pairs of teeth surrounding another ring shunted by an "inductor" made of a long, arc-shaped narrow wire (Figure 1a, b). When the ouroboros was excited on resonance ω_0, the electric field response was strong and tightly confined to the capacitor rings (Figure 1c). The resonance frequency of the ouroboros was determined using the finite element high-frequency simulation solver by ANSYS and experimentally verified using a vector network analyzer. We packaged the sample by suspending it

[1] We used an ouroboros with a double gap designed and fabricated by Wei Fu. It was made by electron-beam lithography etching. The structure is patterned using e-beam lithography patterning of superconducting NbN 40 nm thick on a sapphire wafer 0.5 mm thick.

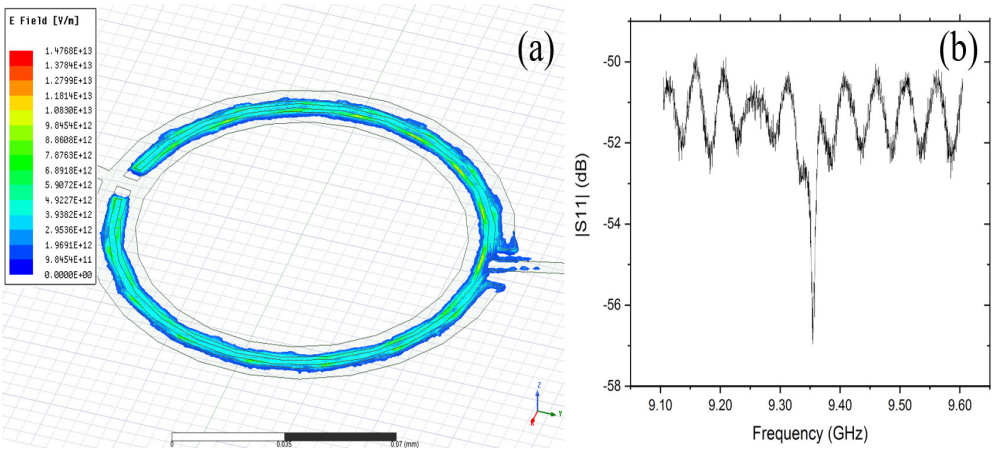

Figure 2. *(a) The simulated ouroboros geometry had a resonance at 9.43 GHz. (b) Experimental characterization agrees with resonance dip at 9.35 GHz. The difference may be attributed to coupling effects in the chamber.*

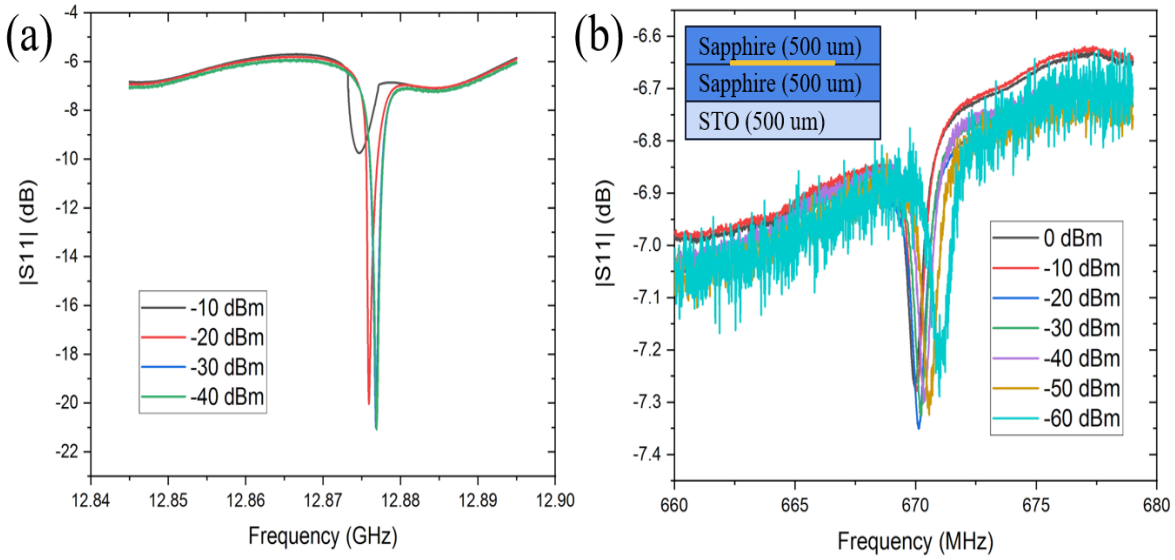

Figure 3. *(a) Duffing nonlinearity of a bare ouroboros with resonant frequency at 12.87 GHz. Higher power shifts the center resonance to lower frequencies, as expected. The quality factor at -40 dBm is 7.3 × 103. (b) STO shifts the resonance frequency much lower, to 670 MHz while still preserving high Q, 9.3 × 102. (Inset diagram: experimental configuration with STO and sapphire spacers)*

on a sapphire holder chip in an air cavity within a copper box. The cavity is probed by a hoop antenna parallel to the capacitor. The sample was cooled below 4 K in liquid helium. The antenna was connected to the VNA, which scanned over the microwave frequencies from 20 MHz to 20 GHz. We measured the reflectance S11 to determine the resonances. On resonance, the locally confined electric field of the ouroboros sample would cause the signal reflectance to sharply dip. The LC resonant frequency is

$$\omega_0 = \frac{1}{\sqrt{LC}}. \quad (1)$$

Inserting a dielectric increases the capacitance by r, thereby decreasing the resonant frequency from its bare value by $1/\sqrt{\varepsilon_r}$. For STO with dielectric constant 11,000, this would mean the resonant frequency would shrink more than 100-fold.

These calculations assume the STO is flush with the superconducting NbN. Due to the complexity of crystal lattice matching in epitaxial growth (see Discussion), the presence of an air gap between the STO wafer and NbN ouroboros printed directly onto sapphire substrate must be taken into consideration. We analyzed the reflection spectrum with either 167 or 500 μm of air gap or sapphire substrate spacing between the sample and resonator. The goal of these different configurations was to distinguish the cavity modes due to the finite nature of the packaging from the actual ouroboros resonance mode. We would be able to tell them apart if we had sufficient coupling between the antenna and the resonator in the presence of STO. We purchased a 5 × 5 × 0.5 mm STO sample from MTI Corporation and probed it using input powers from -60 to 0 dBm to demonstrate the resonator's nonlinear response at higher power (Figure 3). In the presence of STO, this nonlinearity shifts the resonator mode to lower resonant frequencies at higher power, whereas this behavior is the opposite for the cavity modes.

Ultimately, we were unable to definitively recreate the characterization of the specific dielectric value. There were many cavity modes which obfuscated the results since we could not methodically define the coupling of the antenna to the resonator with proper spacing due to different air gaps. Nevertheless, we were able to demonstrate that all the modes were substantially redshifted in the presence of STO. In Figure 3, the unconfirmed mode was shifted by over an order of magnitude due to the high dielectric environment. In addition, this investigation confirmed the very low attenuation of STO since even the cavity mode had a very high quality factor of nearly 10^3, which is key for superconducting delay lines.

SUPERCONDUCTING DELAY LINE DESIGN

Having qualitatively confirmed the characteristics of the STO, we then proceeded to the design of the superconducting delay line. For our delay line, we chose to create a CPW superconducting delay line because it has low spurious modes, high integration level, and easy integration of parallel and series components. (Houdart, 1976) For

the CPW design, I used two different softwares: Sonnet Suites' EM package and ANSYS HFSS. The former performs stacked 2D finite element analysis. This was not only faster, but also allowed for the input of direct kinetic inductance $L_\square$ for the superconducting NbN sheet. The latter calculated full 3D finite element solutions, though it was slow and required input of sheet reactance for the sheet $R_\square$ rather than kinetic inductance, so it was only valid for a single frequency value as

$$R_\square = 2\pi f L_\square .$$

The goal of our CPW line design, again, was to maximize the delay time by slowing down the propagation constant of the signal as much as possible. The propagation constant is

$$v \propto \frac{1}{\sqrt{L'C'}} \quad (2)$$

L' and C' are the values for the effective impedance and capacitance of the line. The value for the propagation constant is reminiscent of the resonant frequency for the LC resonator, presented in Equation 1, though the phenomena are different since here we are dealing with a CPW line. We calculate the propagation constant by varying the length of the line by a small amount Δl, leading to a global phase shift Δl. We use the relation of these variables to calculate the characteristic wavelength of the line which would have the phase go through a full 2π rotation. We multiply this by the frequency, which for reference we take to be 5 GHz across simulations, to get the propagation constant.

$$v = f \cdot 2\pi \frac{\Delta l}{\Delta \phi} \quad (3)$$

In addition to the propagation constant, we record the characteristic impedance to ensure that the delay line, when integrated with other circuit elements, does not suffer from an impedance mismatch. Though we can use impedance matching transformers to translate between different impedances, these will introduce more loss into the system on the order of several dB. Minimizing their use will deliver better results.

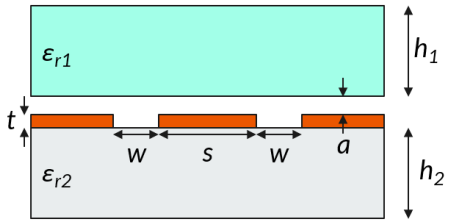

Figure 4. *CPW design parameters.*

There are many parameters which go into CPW design: the dielectric constants ε_{r1} and ε_{r2} below and above the waveguide, corresponding substrate heights h_1 and h_2, CPW thickness t, center patch width s, the gap width w, and air gap a (Figure 4). The below material is sapphire with dielectric constant 11 and thickness 0.5 mm, and the above material is STO with dielectric constant 11,000 and thickness 0.5 mm in our simulations. The thickness of the CPW was fixed to 40 nm and incorporated into the simulation by setting the kinetic inductance at 40 pH/□. Thus, our parameter space spanned the center patch width s, gap width w, and air gap a between the CPW and the above STO crystal.

RESULTS AND DISCUSSION

The optimal CPW delay line that we simulated has 1 μm center width, 1 μm gap width, and no air gap (in the ideal case that the CPW is printed directly onto STO). This CPW has a characteristic impedance of 18 Ω and a propagation constant of 4.2×10^5 m/s or 0.0014c at 5 GHz. This signal propagation is more than 200 times slower than the best superconducting delay line value. If this design is integrated to create a 5 μs delay, then it would only require

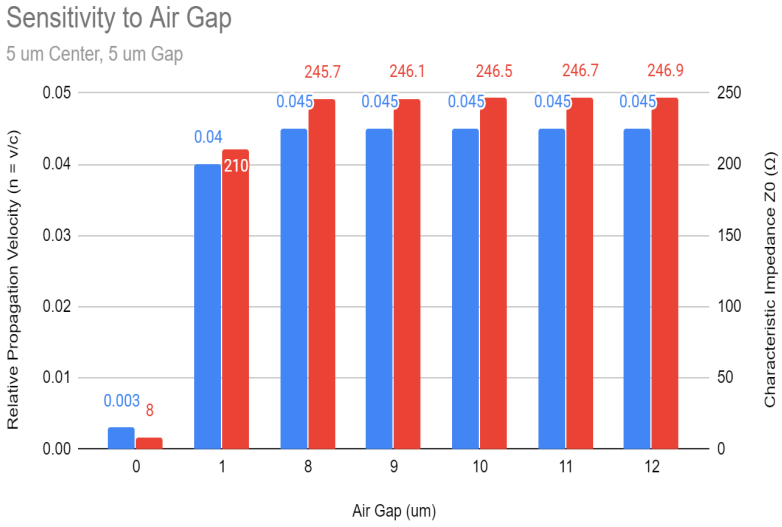

Figure 5. *The CPW is highly sensitive to the existence of the air gap. For any air gap, the propagation constant and characteristic impedance quickly increase. 5 μm center width and 5 μm gap width.*

2.1 m of line. If the line conservatively requires a 20 μm berth for proper in-plane grounding, then it would be able to fit onto 1 cm2 chip with a meander pattern. This very small footprint allows for delay lines to be easily integrated on-chip into microwave systems.

The critical assumption is that there is no air gap. The effect of the high dielectric constant is only relevant if the electric fields of the CPW penetrate deep enough into the STO. However, air readily quenches the electric field, so the behavior of the system is very sensitive to the gap. The elimination of the air gap in practice would require the STO to be epitaxially grown directly on the superconducting resonator substrate. This is certainly possible but makes the fabrication process more difficult. The propagation constant and characteristic impedance quickly jump with any air gap, though once the air gap is opened, these values do not significantly vary (Figure 5). These values are much closer to the values when there was no STO present at all, for which the characteristic impedance is 248 Ω and the propagation constant is 0.045c.

With an air gap present, we further optimized the CPW with different center and gap widths (Figure 6). The propagation constant tends to decrease with a wider center patch. With a larger center width, the capacitance tends to increase because of the effective area of the CPW line. However, this increased width also decreases the kinetic inductance which is proportional to the cross-sectional area of the superconducting material, causing a nonlinear relationship (Figure 6a). The propagation constant does not vary significantly with the gap width (Figure 6b). We would expect that a wider gap would decrease the capacitance and hence increase the propagation constant. We do not see this effect, and it is likely that this is due to the bounds of the simulations' precision or rounding errors in the extraction of the propagation constant, since the characteristic impedance does increase for wider gap widths as expected.

There are still other considerations which this investigation did not explore. We did not factor in attenuation into our simulations, instead assuming that everything was lossless. Dielectric attenuation in a CPW may be approximated as (Pozar, 2009)

$$\alpha_d \approx 4.343 k_0 \frac{\varepsilon_r}{\sqrt{\varepsilon_e}} \frac{(\varepsilon_e - 1)}{(\varepsilon_r - 1)} \tan\delta \quad (4)$$

in dB/m where ε_r is the dielectric constant of STO, ε_e is the effective dielectric constant of the system, and $tan\,\delta$ is the loss tangent. The expression can be simplified considerably since STO has such a large dielectric constant and ε_e may be estimated by $\varepsilon_r/2$. For a 5 GHz signal and with loss tangent of 10^{-3}, the attenuation has an upper bound of 30 dB/m, which would effectively quash the signal. This would need to be confirmed in order to confirm the viability of STO in use for superconducting delay lines. However, by using a more lossless material such as $KTaO_3$, (Krupka et al., 1994) such that loss is less than 2 dB/m, the delay propagation constant may be sacrificed to preserve the signal. In addition, there would need to be further research about the effect that meandering has on the behavior of the line. These investigations were done exclusively with straight lines, meaning that there was no characterization of potential losses due to bends in the wire. Further analysis must be conducted to properly characterize the meandering such that there is no cross-coupling between bends. Lastly, one of the key features of STO is its dielectric voltage tunability. If this is experimentally realized, it may be particularly applicable for expanding the bandwidth of the active superconducting delay line. Elsewhere, this tunability has led to 10-20% variance in the dielectric constant, significantly widening the band for which the device may be usable. (Jackson et al., 1992)

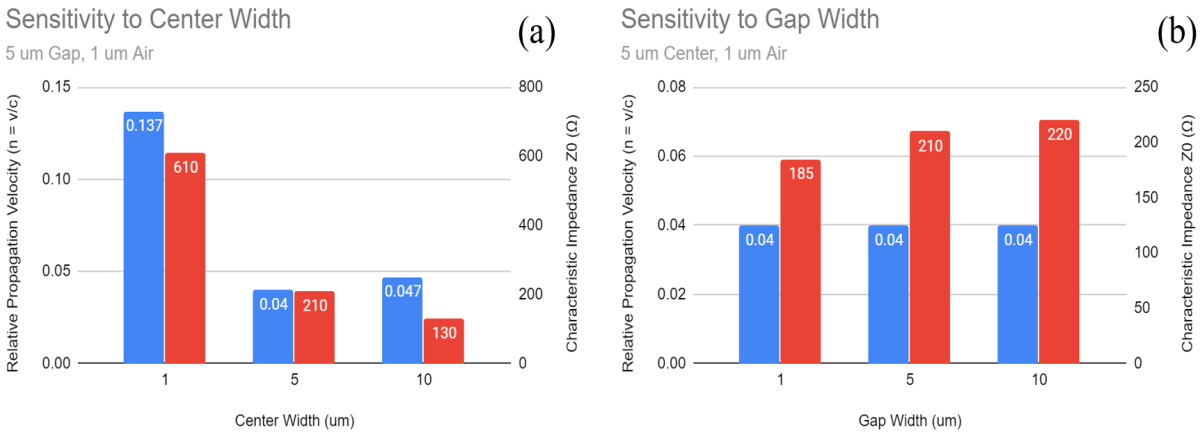

Figure 6. (*a) Sensitivity to center width (reference: 5 μm gap, 1 μm air gap); and (b) sensitivity to gap width (reference: 5 μm center width, 1 μm air gap).*

CONCLUSION

In conclusion, we have presented a design for a coplanar waveguide superconducting delay line enhanced by strontium titanate which achieves a significant improvement in slowing down the propagation constant of microwave signals over previous literature results. STO, with its low loss tangent and extremely high dielectric constant value, may be well-suited for integration into superconducting delay lines. The functionality of this simple design with an STO half-space can be further extended in future research by taking advantage of the voltage tunability of the dielectric constant. The disruptive effect of an air gap means that the fabrication of this device will be complicated by the need for direct growth of STO on the delay line. Nevertheless, this design signals a new realm of research using high-k, low-loss materials which may have promising results. (Krupka et al., 1994) Delays on the order of microseconds can be exploited by experiments which approach the limit of microwave photons' coherence, while the small footprint of this delay device would be useful for microwave filters and integrated microwave photonic design.

REFERENCES

Adam, M., Fuchs, D., & Schneider, R. (2002). YBa2Cu3O7 microwave resonator tuned by epitaxial SrTiO3 thin films. Physica C: Superconductivity, 372, 504-507.

Davidovikj, D., Manca, N., van der Zant, H. S., Caviglia, A. D., & Steele, G. A. (2017). Quantum paraelectricity probed by superconducting resonators. Physical Review B, 95(21), 214513.

Findikoglu, A., Jia, Q., Wu, X., Chen, G., Venkatesan, T., & Reagor, D. (1996). Tunable and adaptive bandpass filter using a nonlinear dielectric thin film of SrTiO3. Applied physics letters, 68(12), 1651-1653.

Han, X., Zou, C.-L., & Tang, H. X. (2016). Multimode strong coupling in superconducting cavity piezoelectromechanics. Physical review letters, 117(12), 123603.

Hattori, W., Yoshitake, T., & Tahara, S. (1999). A Superconducting Delay-Line Memory Using a YBa 2 Cu 3 O 7-δ Coplanar Line. In Advances in Superconductivity XI (pp. 1263-1266): Springer.

Hohenwarter, G., Track, E., Drake, R., & Patt, R. (1993). Forty five nanoseconds superconducting delay lines. IEEE Transactions on Applied Superconductivity, 3(1), 2804-2807.

Houdart, M. (1976). Coplanar lines: Application to broadband microwave integrated circuits. Paper presented at the 1976 6th European Microwave Conference.

Huang, F. (1997). Thin-Film HTS delay-line filters. Cryogenics, 37(10), 671-679.

Jackson, C. M., Kobayashi, J. H., Lee, A., Pettiette-Hall, C., Burch, J. F., Hu, R., . . . McDade, J. (1992). Novel monolithic phase shifter combining ferroelectrics and high temperature superconductors. Microwave and Optical Technology Letters, 5(14), 722-726.

Kapolnek, D. J., Aidnik, D., Hey-Shipton, G., James, T., Fenzi, N., Skoglund, D., & Nilsson, B. (1993). Integral FMCW radar incorporating an HTSC delay line with user-transparent cryogenic cooling and packaging. IEEE Transactions on Applied Superconductivity, 3(1), 2820-2823.

Krupka, J., Geyer, R. G., Kuhn, M., & Hinken, J. H. (1994). Dielectric properties of single crystals of Al/sub 2/O/sub 3/, LaAlO/sub 3/, NdGaO/sub 3/, SrTiO/sub 3/, and MgO at cryogenic temperatures. IEEE transactions on microwave theory and techniques, 42(10), 1886-1890.

Liang, G.-C., Shih, C.-F., Withers, R. S., Cole, B. F., & Johansson, M. E. (1996). Space-qualified superconductive digital instantaneous frequency-measurement subsystem. IEEE transactions on microwave theory and techniques, 44(7), 1289-1299.

Müller, K. A., & Burkard, H. (1979). SrTi O 3: An intrinsic quantum paraelectric below 4 K. Physical Review B, 19(7), 3593.

Pozar, D. (2009). Microwave engineering. Michigan. In: Wiley.

Rigetti, C., Gambetta, J. M., Poletto, S., Plourde, B., Chow, J. M., Córcoles, A., . . . Keefe, G. A. (2012). Superconducting qubit in a waveguide cavity with a coherence time approaching 0.1 ms. Physical Review B, 86(10), 100506.

Sakudo, T., & Unoki, H. (1971). Dielectric Properties of SrTi O 3 at Low Temperatures. Physical review letters, 26(14), 851.

Su, H. T., Wang, Y., Huang, F., & Lancaster, M. J. (2008). Superconducting delay lines. Journal of superconductivity and novel magnetism, 21(1), 7-16.

Talisa, S., Janocko, M., Meier, D., Moskowitz, C., Grassel, R., Talvacchio, J., . . . Pieseski, S. (1995). High-temperature superconducting wide band delay lines. IEEE Transactions on Applied Superconductivity, 5(2), 2291-2294.

STEM